2026 IEEE International Conference on Robotics and Automation (ICRA 2026)
June 1-5, 2026. Vienna, Austria

Proposal of an Embodied Airbag-Pressure-Based Control Interface for Inflatable Personal Mobility Devices

Reon Hayami, Bill Falk, Takuya Sasatani, *Member*, *IEEE*, Shigeki Sugano, *Fellow*, *IEEE*, and Mitsuhiro Kamezaki, *Member*, *IEEE*

***Abstract*—The demand for personal mobility devices (PMDs) has increased, prompting studies on various control interfaces such as joysticks and handlebars. However, these interfaces remain external to the PMD, and no system has been developed in which the PMD itself functions as the interface. This study proposes an interface that measures and controls the internal air pressure of an inflatable PMD, enabling the system to recognize operator inputs, such as pressing, leaning, or pushing, directly from the PMD body. The system adjusts air pressure according to the operator's estimated weight, allowing operation with minimal force, while continuous speed control is realized through *press*, *lean*, and *double-push* inputs. Experimental results demonstrated that translational and angular speeds could be controlled through embodied body movements, and filter processing effectively mitigated the influence of air pressure fluctuations caused by uneven terrain, ensuring stable operation. Tests conducted on indoor and outdoor courses, including obstacles and uneven surfaces, showed operability comparable to a joystick, though narrower paths required more time to navigate. This study contributes a novel embodied air-pressure-based control paradigm that directly integrates the interface into the PMD itself.**

I. Introduction

PERSONAL mobility devices (PMDs) have been extensively studied, driven by increasing demand not only as elderly transportation but also as last-mile solutions in urban areas and tourist destinations. PMDs must operate in pedestrian-shared environments such as sidewalks and stores, both indoors and outdoors. To meet these demands, various forms of PMDs have been developed, including electric wheelchairs [1], electric scooters [2], and inverted pendulum types [3]. Among them, "Poimo" features an inflatable structure that expands with air, providing a soft body compared to metal-based designs [4]–[6]. Because most of its body consists of airbags, Poimo is soft and lightweight yet sufficiently rigid to support a person. When deflated, it becomes compact and easy to carry (the lower right of Fig. 1(a)). Its soft body also reduces the risk of injury in collisions with people or obstacles, enhancing safety in physical contact.

On the other hand, studies on human-machine interfaces for PMD control have also been actively conducted, including joysticks [7], [8] and handlebars [2], [9]. PMDs are used for various purposes, so their interfaces requirements also vary: ease of use for elderly or physically challenged users [10], [11], intuitiveness for beginners [11], [12], and prioritization of safety [4]. However, these interfaces are not integrated into the PMD itself, requiring separate control units that must be attached to the PMD. They may also need to be replaced depending on the operator's attributes, and additional effort is required to learn how to use them.

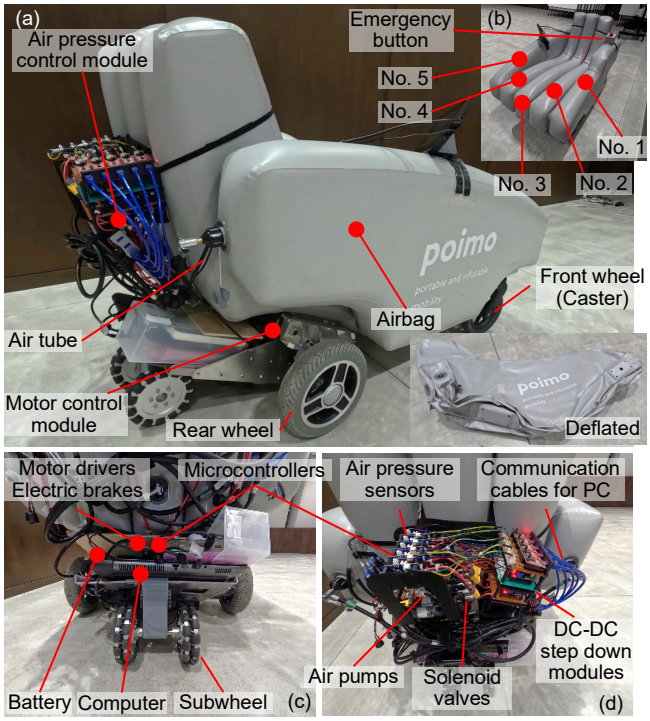

Fig. 1. Inflatable soft mobility equipped with air pressure and motor control modules: (a) side view, (b) front view, (c) motor control module, and (d) air pressure control module.

To address this issue, we propose a system in which the PMD itself functions as the control interface that interprets the operator's input through its own body as a sensing medium. As a feasibility study of an embodied airbag-pressure-based control interface for inflatable PMDs, we employ Poimo, as shown in Fig. 1(a). The operator intuitively uses body movements, such as *pressing*, *leaning*, and *pushing*, and the system recognizes these embodied input actions from airbag pressure changes and controls the PMD, as shown in Fig. 2.

II. Related Works

1) Interfaces for PMDs: A variety of interfaces have been

This research is part of the results of Value Exchange Engineering, a joint research project between Mercari R4D Lab and RIISE (Research Institute for an Inclusive Society through Engineering). This work was also supported in part by the Waseda Research Institute for Science and Engineering and the Future Robotics Organization, Waseda University.

R. Hayami and S. Sugano are with the Depart. Modern Mechanical Engineering, Waseda Univ., 17 Kikui-cho, Shinjuku-ku, Tokyo 162-0044, Japan.

B. Falk is with the Depart. Information Technology, Chalmers University of Technology, Chalmers tekniska högskola AB, 412 96 Göteborg, Sweden

T. Sasatani and M. Kamezaki is with the Graduate School of Engineering, The University of Tokyo, 7-3-1 Hongo, Bunkyo-ku, Tokyo 113-8656, Japan. (e-mail: kamezaki@akg.t.u-tokyo.ac.jp)

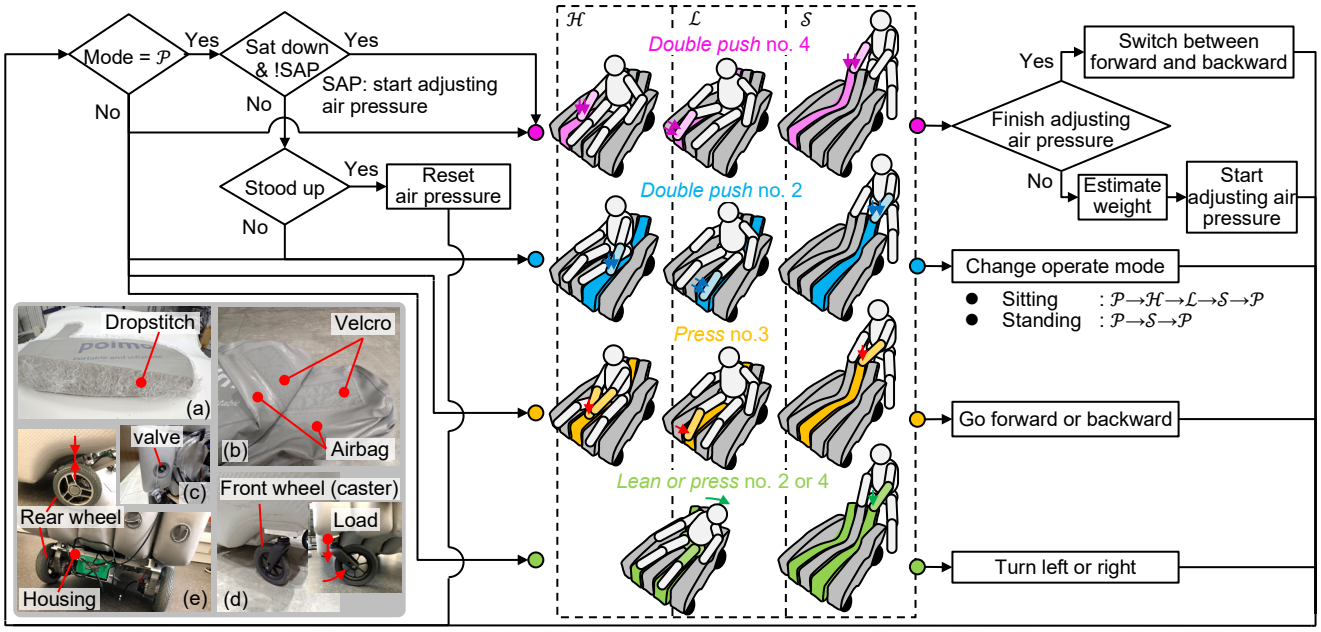

Fig. 2. Overview of proposed system. Operator sits on PMD. After double-push on no. 4, system estimates operator's weight from airbag pressure changes and adjusts air pressure accordingly to minimize require input force. Following adjustment, operator double-pushes no. 2 and selects control mode. Then, operator controls PMD by performing input actions. Before standing up, operator switches to $\mathcal{P}$; once standing, airbag pressure resets to default value, returning system to its initial state. For $\mathcal{S}$, air pressure adjustment is skipped and operation begins directly. Inflatable personal mobility device "Poimo": (a) internal structure, (b) inter-airbag connection, (c) air valve, (d) front wheel, and (e) rear wheel.

studied for different user groups. In the leg-operated interface [10], driving, stopping, and turning are intuitively controlled by combinations of the left and right pedal presses. In the head-operated interface [11], a device attached to the head detects the user's facing direction, and translational and angular velocities are controlled by the pitch and roll angles, enabling operation even for users unable to use their hands or legs. In an interface using the body's center of gravity (CoG) [12], the PMD detects the upper body's CoG in a standing posture and moves in the leaning direction, allowing intuitive control without hands or legs. As a soft interface, a sensor made of conductive urethane foam was developed to detect multimodal inputs, such as pressing or pinching, with a single sensor [13], and a PMD interface was proposed in which the device responds differently depending on user's action: pressing, gripping, or touching [4]. However, these interfaces are independent and are not integrated with PMDs.

2) Pressure-based interface: Air pressure has also been explored as an interface modality. By detecting and controlling the pressure inside an airbag, input can be recognized and shape change achieved with a simpler structure than electronic components [14]. In an interface [15], air flows through a hollow object with multiple holes of varying diameters; pressure variations at different hole positions enables recognition of both touch and position. In smartphone interfaces [16], multiple airbags are arranged to recognize actions, such as press, pinch, and pull, based on the air pressure changes in each airbag. Nevertheless, these approaches remain independent. In an airbag pillow interface [17], head movements are detected as pressure changes and used for tasks, such as controlling a mouse cursor. Although not intended for PMD control, the pillow itself functions as an input device. Similarly to this concept, our study proposes extending the integration of interface functionality directly into the PMD body for control.

III. Design Concept and Equipment

In this section, we describe the PMD structure, concept of the proposed interface, and air pressure control system.

A. Inflatable soft mobility Poimo

As shown in Fig. 1, Poimo is an inflatable PMD whose body is formed by filling the airbags with air through a valve (Fig. 2(c)). The internal structure employs a dropstitch design that maintains shape under pressure, allowing the PMD to support a person (Fig. 2(a)). The body consists of five horizontally-aligned airbags, which are referred to as nos. 1–5 from left to right (Fig. 1(b)), each connected via Velcro (Fig. 2(b)). The front wheels are casters independently attached to nos. 1 and 5. They are unstable because each is connected to a single airbag (Fig. 2(d)). If the airbag pressure is low or a heavy load is applied, the caster may fail to remain upright, preventing movement. The rear wheels are tires connected by a rigid housing attached to nos. 2 and 4 (Fig. 2(e)). When the airbag pressure is low or a heavy load acts on the casters, the rear wheels may interfere with nos. 1 and 5. Moreover, since the wheels and airbags are interconnected, forces from the road surface during operation also affect the internal air pressure of the airbags.

B. Air pressure and motor control system

Fig. 3 shows an overview of the air pressure and motor control system. Five air pressure sensors (MP3V5050GP, NXP USA; 0–50 kPa) were installed to measure the airbag pressure and recognize operator input. The default pressure of 44100 Pa used in the previous papers [4]–[6] was too rigid to recognize the operator actions. Thus, the airbag pressure is set as low as possible depending on the situation (explained later).

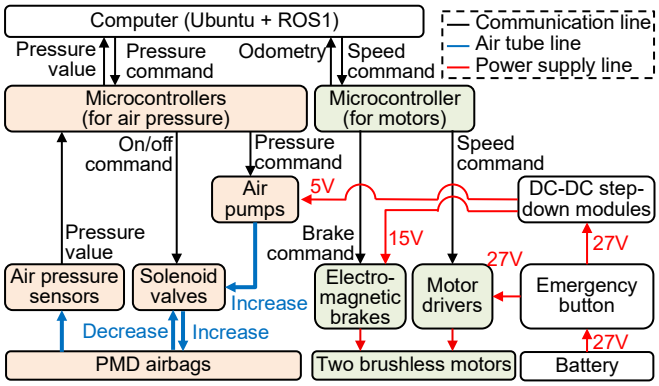

Fig. 3. Overview of air pressure and motor control system.

To control the airbag pressure, five air pumps (MAP-AM-265, Minebea; max 53.3 kPa, 1.03 l/min) and solenoid valves (S070C-VAG-32, SMC; max 300 kPa) were installed. These components are connected to the airbags via hoses and controlled by a microcontroller (STM32L412K8, STMicroelectronics). The system appearance is shown in Fig. 1(d). A laptop computer running Ubuntu and ROS manages the entire system and communicates with microcontrollers for air pressure and motor control. For the PMD's motor control, the motor microcontroller controls the motor drivers and electromagnetic brakes, operating two brushless motors (Fig. 1(c)).

C. Concept of airbag-pressure-based embodied interface

Our approach eliminates the need for an external interface by utilizing the PMD's body itself as the control medium. As shown in Fig. 2, the system detects operator inputs through air pressure changes and applies them for PMD control.

1) Control modes: The system provides four control modes: hands $\mathcal{H}$ or legs $\mathcal{L}$ while seating, or hand while standing $\mathcal{S}$, and parking $\mathcal{P}$. The entire PMD airbags serve as an input interface, so unintended movement must be prevented when the airbag is touched without intent to control. In $\mathcal{P}$, the PMD remains stationary, thereby avoiding unintended inputs during free movements such as repositioning. $\mathcal{H}$, $\mathcal{L}$, and $\mathcal{S}$ are selected according to operating conditions. $\mathcal{H}$ is used when the operator is seated and presses the airbag with their hands. $\mathcal{L}$ is used when the hands are unavailable (e.g., occupied with luggage), enabling leg operation. $\mathcal{S}$ is used when the PMD is controlled from behind, as in caregiver operation similar to pushing a wheelchair.

2) Input actions: The interface employs three input actions: *press or lean* (continuous force) and *push* (momentary force). *Pressing* with the hands or legs is recognized as an analog input proportional to the applied force. Maintaining continuous pressure can be physically demanding, so this action is preferably assigned to no. 3 (low pressure). *Leaning* the body to left or right is also recognized as an analog input, proportional to the degree of lean. *Leaning* is less demanding than *pressing*, as it relies on body weight rather than applied force. *Pushing* is less demanding still than *pressing* and is treated as a binary action (performed or not), recognized as a digital input.

The proposed control methods are summarized in Table I. Translational speed is controlled by *pressing* no. 3, with either hand or leg. Stronger *press* results in higher speed. Angular speed is controlled by *leaning* the body or *pressing* nos. 2 and 4 with the hand. Greater *leans* or *presses* produce higher angular speeds. To prevent false recognition, in this study, *push* requires two consecutive actions (*double-push)* to register. *Double-push* on no. 2 switches the operation mode cyclically among $\mathcal{P}$, $\mathcal{H}$, $\mathcal{L}$, and $\mathcal{S}$. *Double-push* on no. 4 toggles the travel direction between forward and backward, and after sitting on the PMD, also initiates air pressure adjustment.

TABLE I
OPERATOR INPUT ACTIONS AND INTERFACE RESPONSES

Position	Input action	Interface response
No. 3	*Press*	Control translational speed. Pressure ∝ speed.
Nos. 2/4	*Lean* or *Press*	Control angular speed. Pressure ∝ speed.
No. 2	*Double-push*	Change operate mode.
No. 4	*Double-push*	Switch travel direction/Start air pressure adjustment.

IV. Development of Inflatable Interface System

This section describes the overall of the proposed inflatable interface system, including the details of the air pressure control, operation methods, and speed control.

A. Airbags used for interface and preset air pressure

Input actions change the airbag pressure, and the system recognizes these changes as input signals. The magnitude of pressure changes depends on the preset air pressure before pressing. Fig. 4 shows the pressure variations for different preset values when force is applied. While greater force produces larger pressure change, lower preset pressures yield sensitivity to the same applied force. To effectively use air pressure changes as an interface, input should be recognized with minimal force. Thus, the preset pressure should be as low as possible so that small forces generate significant pressure changes. However, if the preset pressure is too low, the PMD may lack sufficient rigidity to certain body weight, or the airbag may fail to recover its shape after being pressed. We experimentally determined the lowest preset air pressures that satisfy the following three conditions.

1) Shape maintenance during control: The PMD must maintain its shape such that the front casters do not collapse, ensuring operability, and the rear wheels do not contact nos.1 and 5. Since the front casters are independently connected, nos. 1 and 5 require higher pressure. In contrast, nos. 2 and 4 are connected to the housing linking the rear wheels, providing stability and allowing shape retention even at lower pressures. No. 3 minimally contributes to structural support and can thus be to set the lowest pressure. Accordingly, no. 3 is kept as soft as possible, while nos. 1 and 5 are excluded from use as an input interface and set to the maximum pressure of 44100 Pa. From exploratory experiments, we determined the minimum pressures required for nos. 2, 3, and 4 at each body weight, as shown by the black plots in Fig. 5.

2) Airbag recovery after pressing: For repeated input, the airbag must return to its original shape after being pressed. We experimentally found that the recovery failed at pressure below 750 Pa, as indicated by the green lines in Fig. 5.

3) Robustness to weight estimation error: The system estimates the operator's weight to expand the input pressure range, but estimation error may occur. A margin is thus

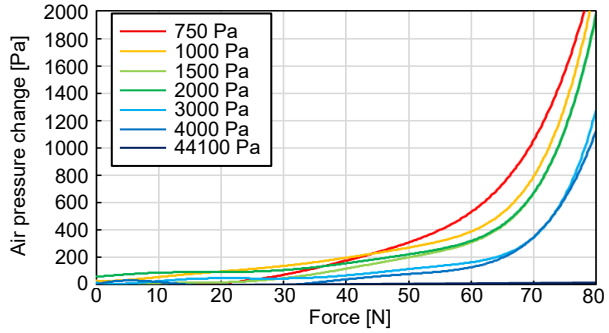

Fig. 4. Relationship between applied force and air pressure change.

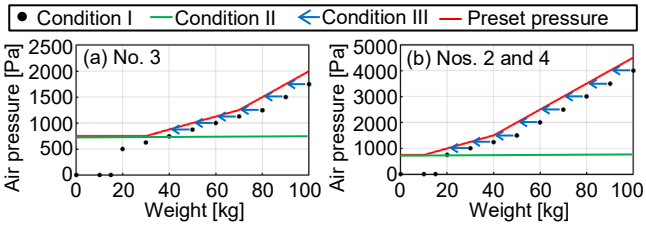

Fig. 5. Preset air pressures for each airbag. Relationship between operator's weight and minimum air pressure.

required to satisfy the above conditions even when weight is overestimated. As detailed later, the maximum estimation error was 5.63 kg. Thus, a margin of 10 kg was applied to ensure robustness, as shown by the blue arrows in Fig. 5.

Finally, the preset air pressures for no.3 and nos. 2 and 4 are determined as indicated by the red lines in Fig. 5.

B. Default pressure for each airbag and weight estimation

The system first determines the default pressure and estimates the operator's weight to minimize the airbag pressure.

1) Default pressure: Even for operators of the same weight, the magnitude of pressure change varies with the initial pressure before sitting. Thus, the default pressure for each airbag P^1_{def}, P^2_{def}, P^3_{def}, P^4_{def}, and P^5_{def} are determined prior to sitting. In this study, the requirement is that the PMD shape must be maintained even under a load of 100 kg (a heavyweight person). PMD movement is unnecessary, so only shape retention in a stationary state was verified. Based on experiments, the default pressures were set to P^3_{def} = 750 Pa, $P^2_{def} = P^4_{def}$ = 1500 Pa, and $P^1_{def} = P^5_{def}$ = 44100 Pa.

2) Weight estimation: The estimated weight $\hat{w}$ is obtained using a regression equation derived from training data of pressure changes for each weight while sitting. Specifically, we measured 10 times for each body weight of 15, 30, 50, 60, 70, 80, 90, and 100 kg, resulting in a total of 80 data points. The regression equation is expressed as

$$\hat{w} = \alpha_0 + \sum_{k=1}^{5} \alpha_k \delta P^k \quad , \tag{1}$$

where k is the number of airbags (1–5), δP^k is the pressure change of each airbag, α_0 and α_k is the regression coefficient. After training, we obtained α_0 = 13.259, α_1 = 0.000, α_2 = 0.013, α_3 = 0.008, α_4 = 0.026, and α_5 = 0.000.

C. Baseline pressure and input action recognition

We describe the method for recognizing operator input action based on changes in air pressure.

1) Baseline pressure: A baseline pressure must be defined

TABLE II
AIR PRESSURE FLUCTUATION RANGE IN STEADY STATE

Weight kg	Standard deviation Pa			Max fluctuation range Pa		
	no. 2	no. 3	no. 4	no. 2	no. 3	no. 4
60	11.7	15.5	20.7	32.1	62.4	88.6
70	19.3	12.3	12.5	50.6	51.6	63.3
80	12.4	14.4	20.0	22.6	56.5	77.3

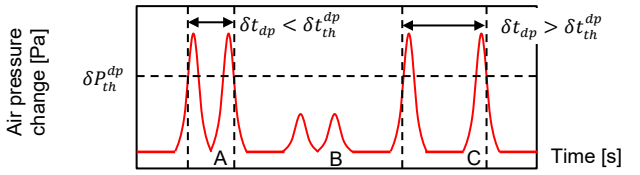

Fig. 6. Time-series change in air pressure during double-push. A: detected double-push, B: pressure change smaller than δP^{dp}_{th}, and C: not detected as double-push as double-push time δt_{dp} is longer than δt_{th}.

to compare air pressure change when force is applied to the airbag. Ideally, it should match the preset pressure based on the operator's weight, as defined in Fig. 5. However, posture change of the operators during operation may cause deviations in action recognition, so the baseline pressure must be periodically updated. When updating, it must correspond to a steady state where no input is applied, requiring the system to recognize non-operation states. Table II lists the fluctuation range and standard deviation of air pressure measured for 30 s at various body weights. The results indicate that body weight had no effect, and the pressure fluctuated within ±100 Pa with a standard deviation below 25 Pa. Accordingly, we defined the steady state as the condition where the PMD is stationary and the standard deviation of the time-series pressure data in 2 s is 25 Pa or less. The pressure at this steady state is used as the baseline pressure. To allow immediate adaptation, and this process is repeated every 2 s.

2) Double-push recognition: The *double-push* for nos. 2 and 4 is recognized by analyzing the time-series pressure. As shown in Fig. 6, a *double-push* is detected when the pressure exceeds the threshold δP^{dp}_{th} twice within a specified interval, set to prevent false recognition. In this study, δt^{dp}_{th} was set to 1.0 s, and δP^{dp}_{th} to 350 Pa for a 60-kg operator. Since the *double-push* is intended only when the PMD is stationary, recognition is limited to stationary conditions.

3) No. 3 press recognition: Press is detected when the air pressure change δP^3 falls between the minimum δP^3_{-th} and maximum threshold δP^3_{+th}. Once detected, the normalized air pressure change $\delta P^3_{norm} \in [0, 1]$ is calculated as

$$\delta P^3_{norm} = (\delta P^3 - \delta P^3_{-th})/(\delta P^3_{+th} - \delta P^3_{-th}) \quad , \tag{2}$$

and used as a control input.

- *Lower threshold δP^3_{-th}:* It must exceed the steady-state fluctuation range to prevent false press recognition. Considering the maximum fluctuation of 100 Pa (Table II), we set δP^3_{-th} > 100 Pa. Fig. 7 shows the pressure changes when a 60-kg operator uses a joystick to move forward, backward, and turn. Because the applied force direction depends on the front caster orientation, which varies with both PMD movement and road conditions, it is unpredictable. Thus, the threshold must prevent false detection regardless of caster orientation. As shown in Fig. 7, the pressure changes in no. 3 remain below 250 Pa for a 60-kg

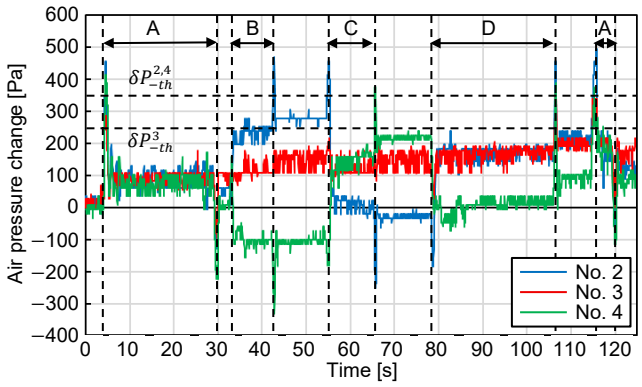

Fig. 7. Air pressure changes caused by caster orientation during operation. A: forward, B: turn left, C: turn right, and D: backward.

TABLE III
UPPER AND LOWER PRESSURE THRESHOLD FOR PRESS AND LEAN

Weight kg	δP^{3}_{-th} Pa	δP^{3}_{+th} Pa	$\delta P^{2,4}_{-th}$ Pa	$\delta P^{2,4}_{+th}$ Pa
60	250	800	350	700
70	250	800	400	750
80	250	800	450	800

operator. We thus set δP^{3}_{-th} = 250 Pa, corresponding to the pressure change produced by around 50 N at a preset pressure of 1000–2000 Pa (yellow and green lines in Fig. 4).

- *Upper threshold* δP^{3}_{+th}*:* A higher δP^{3}_{+th} facilitates speed adjustment but requires more force to reach high speeds. Conversely, a lower value enables high speeds with less force but reduces speed controllability. Thus, we set δP^{3}_{+th} = 800 Pa, corresponding to the pressure change produced by around 70 N at a preset pressure of 1000–2000 Pa (yellow and green line in Fig. 4). Compared with δP^{3}_{-th}, a margin of 20 N was considered sufficient for operation.

We summarized the lower and upper thresholds for 60, 70, and 80 kg in Table III.

4) Nos. 2 or 4 lean/press recognition: Fig. 8 shows the air pressure change when the body is leaned to the left or right. The roll angle of the body was measured using an inertia measurement unit (IMU) (ZED2i, StereoLabs) placed on the abdomen while seated on the PMD. As the lean angle increases, the pressure on the leaning side rises, while the pressure on the opposite side decreases as the buttocks lift off the airbag. Once the buttocks completely leave the airbag, however, the pressure no longer changes. Thus, only the increase in pressure is used to measure the amount of lean. Based on this, when the pressure change of nos. 2 or 4 $\delta P^{2,4}$ falls between the minimum $\delta P^{2,4}_{-th}$ and maximum threshold $\delta P^{2,4}_{+th}$ while the opposite side decreases, the system determines that the body is leaning toward the side of the increasing pressure. The normalized pressure change $\delta P^{2,4}_{norm}$ is then calculated as

$$\delta P^{2,4}_{norm} = (\delta P^{2,4} - \delta P^{2,4}_{-th})/(\delta P^{2,4}_{+th} - \delta P^{2,4}_{-th}) \ . \quad (3)$$

We set the turning initiation and maximum lean angles to 5° and 15°. From Fig. 7, we determined $\delta P^{2,4}_{-th}$ = 350 Pa for a 60 kg operator (≈ 5°) and $\delta P^{2,4}_{th+}$ = 700 Pa for a 60 kg operator (≈ 15°). Similarly, we summarized the lower and upper thresholds for 60, 70, and 80 kg in Table III.

D. Speed control

1) Translational speed: The translational speed command value v_c is calculated as

$$v_c = \delta P^{3}_{norm} \cdot v_c^{max} \ , \quad (4)$$

where v_c^{max} is the maximum speed. For forward movement, it is set to 1.111 m/s (= 4 km/h), similar to human walking speed. For backward movement, it is set to 0.556 m/s (= 2 km/h), half of the forward speed.

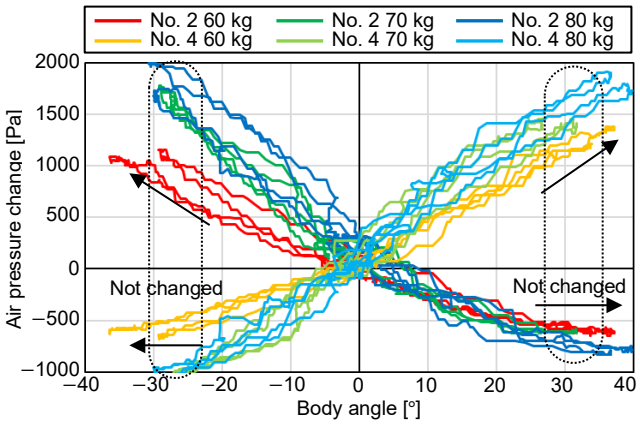

Fig. 8. Relationship between body angle and air pressure change.

2) Angular speed: The angular speed command value ω_c is calculated as

$$\omega_c = \delta P^{2,4}_{norm} \cdot \omega_c^{max} \ , \quad (5)$$

where ω_c^{max} is the maximum speed. For forward movement, it is set to 47.7 °/s (=3000 rad/h), similar to human rotation speed. For backward movement, it is set to 31.8 °/s (= 2000 rad/h), two-thirds of the forward speed.

3) Filtering: To ensure stable operation, two filters are applied to v_c and ω_c. The first is a low-pass filter that applies 2-s moving average to smooth air pressure fluctuations and variations in applied force. The second is an acceleration limiter that suppresses sudden speed changes caused by misoperation or when overcoming steps. In this study, the acceleration limit is set to 0.3 m/s^2 under normal conditions. However, when the command value is 0 and the PMD is stopping, the limit is relaxed to 0.5 m/s^2 to handle emergencies, such as avoiding collisions with obstacles.

4) Electromagnetic brake: The brake is activated when both v_c and ω_c remain 0 for a specified period Δt^b. It is released once either v_c or ω_c becomes non-zero. Introducing a short delay before brake activation allows the PMD to continue moving and decelerate naturally due to inertia. While this reduces responsiveness, it softens deceleration during unintended release of *press* and enables smoother speed control. Δt^b is set to 2.5 s, as the PMD requires around 2 s to stop from v_c^{max} due to inertia.

V. SYSTEM VERIFICATION EXPERIMENTS

We conducted verification experiments for each system to ensure that the proposed system operates correctly.

A. Weight estimation

The accuracy of the body weight estimation was evaluated. Fig. 9 shows the estimated weights when operators weighing 60, 70, and 80 kg each boarded the PMD five times. The

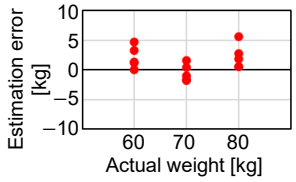

Fig. 9. Result of weight estimation.

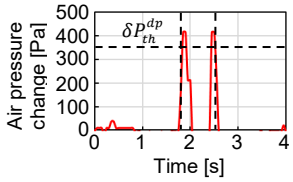

Fig. 10. Pressure change in double-push.

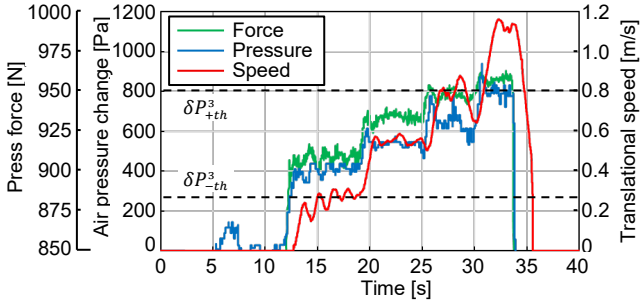

Fig. 11. Force, air pressure, and translational speed during pressing no. 3.

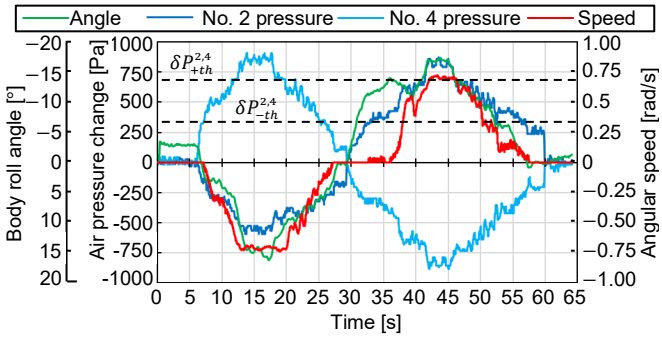

Fig. 12. Body angle, air pressure, and angular speed during leaning.

maximum error was +5.63 kg, the root mean square error (RMSE) was 2.43 kg, and the mean error was 1.858%. Due to the maximum error, the preset air pressure varies by up to around +141 Pa for no. 3 and around +282 Pa for nos. 2 and 4, as shown in Fig. 5. These variations in stiffness remained within an acceptable range for *press* or *lean* operations.

B. Change mode and speed control

1) Change mode: The pressure waveform during *double-push* was verified. As shown in Fig. 10, the pressure exceeds the threshold twice within a specified period.

2) Translational speed: The PMD was operated by *pressing* no. 3 with the hand at four levels of increasing force. The traveling speed was recorded when the airbag was pressed through a pressure sensor sheet (FSR406B, Interlink Electronics). Fig. 11 shows the relationship between the pressing force, pressure change, and actual speed. As the pressing force increased, the pressure change also increased. When the pressure change exceeded δP^3_{-th}, the PMD started moving. By setting the pressure threshold between 250 and 800 Pa, speed could be adjusted across four levels: around 0.28, 0.56, 0.83, and 1.11 m/s.

3) Angular speed: The PMD was operated by leaning the body. Using an IMU placed on the abdomen, the pressure and speed corresponding to the body angle were recorded. Fig. 12 shows the body angle, pressure change, and actual angular speed during leaning. As the body angle increased and the air pressure exceeded the threshold, angular speed is generated,

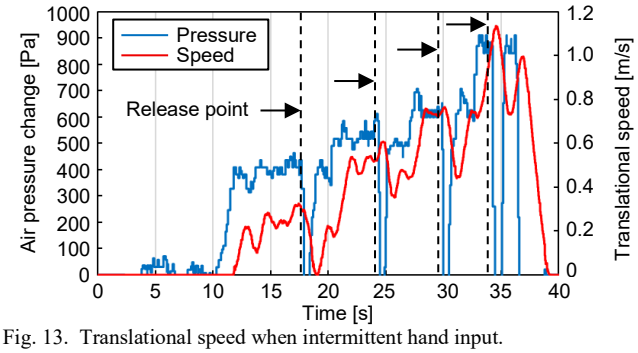

Fig. 13. Translational speed when intermittent hand input.

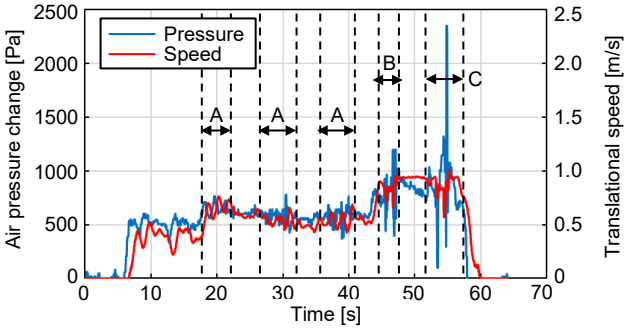

Fig. 14. Translational speed. A: tactile paving, B: 2cm step, C: 3cm step.

with further increases in pressure producing higher angular speed.

C. Smooth speed control under intermittent pressing

The PMD was operated at four different speed levels, during which the hand was momentarily released and then reapplied. Fig. 13 shows the speed response when force is temporarily released. At around 0.2 m/s, releasing force reduced the speed to 0, stopping the PMD. At higher speeds, instead of applying the electromagnetic brake immediately when both the air pressure change and speed command dropped to 0, a 2.5 s interval period of movement by inertia was introduced, preventing a complete stop. This brake control reduces sudden deceleration when the force was temporarily released.

D. Robust control during uneven road traveling

The PMD was tested over tactile paving and steps, as shown in Fig. 15(a). Fig. 14 shows the changes in air pressure and speed when driving over tactile paving and steps of 2 and 3 cm height. On tactile paving, surface unevenness caused small pressure fluctuations, which were smoothed by the low-pass filter. When crossing steps, the airbag was rapidly pressurized as the wheels transmitted the impact of the steps, but the acceleration limiter suppressed sudden acceleration.

VI. Experiment and Discussion

We conducted driving experiments to verify whether the system operates as intended in various environments.

A. Method and evaluation

1) Course: Three courses were used to evaluate the proposed method (Fig. 15). The first is an indoor course with obstacles, including an S-curve, tactile paving, and steps (Fig. 15(a)). The second is an outdoor grassy path with straight sections and turns (Fig. 15(b)). The third is an indoor sloped path

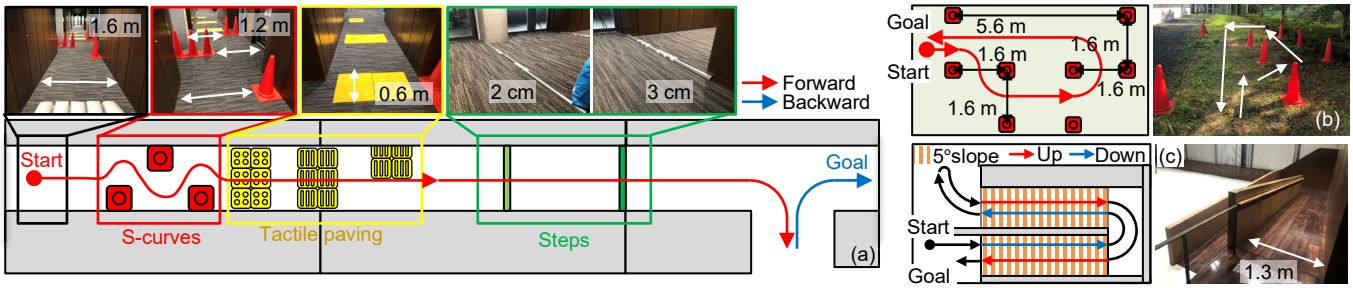

Fig. 15. Experiment course layout (top view). (a) Course 1: S-curves, tactile paving, and steps, (b) Course 2: grassy path, and (c) Course 3: sloped path.

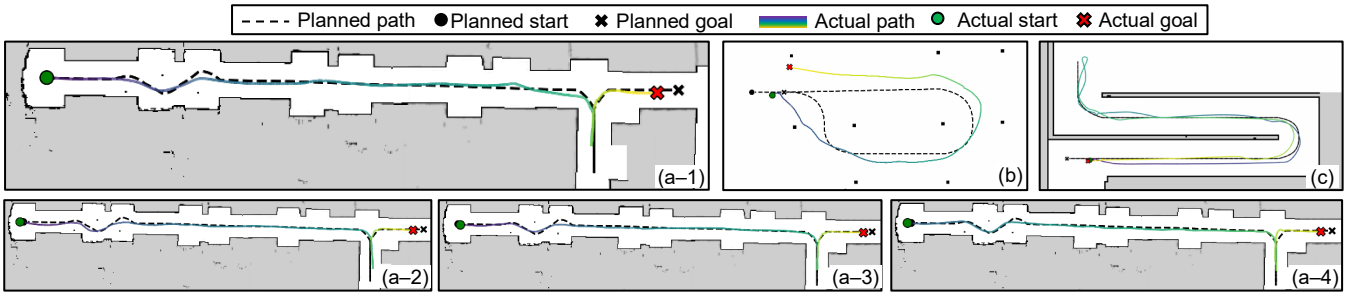

Fig. 16. Target and actual travel paths. (a-1) Course 1 $\mathcal{H}$, (a-2) Course 1 $\mathcal{L}$, (a-3) Course 1 $\mathcal{S}$, (a-4) Course 1 $\mathcal{J}$, (b) Course 2, and (c) Course 3.

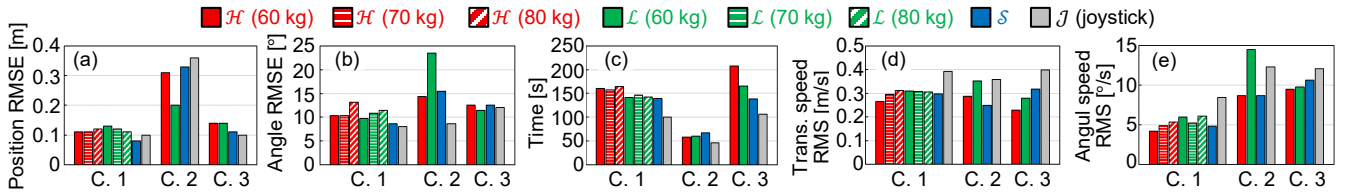

Fig. 17. Experimental results. (a) Positional RMSE, (b) angular RMSE, (c) travel time, (d) translational speed RMS, and (e) angular speed RMS.

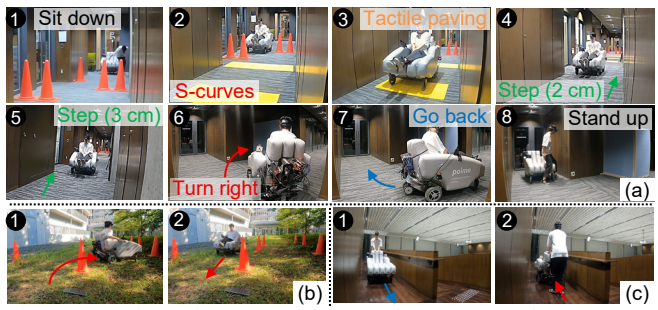

Fig. 18. Experimental scenes. (a) Course 1, (b) Course 2, and (c) Course 3.

with a 5° incline, where the PMD descends, turns, and then ascends (Fig. 15(c)). Each course was tested in three control modes hand ($\mathcal{H}$), leg ($\mathcal{L}$), and standing ($\mathcal{S}$). Driving with a joystick ($\mathcal{J}$) was also included for comparison.

2) Evaluation metrics: 60, 70, 80-kg operators control the PMD, and the trajectories on each course were recorded. Operability was evaluated using the root mean square error (RMSE). The trajectory was measured with two 2D LiDARs mounted on the side of the PMD (Fig. 1), recording trajectory points at 20 Hz. The positional RMSE was calculated as the minimum Euclidean distance between each trajectory point and the target path. The angular RMSE was calculated as the angular difference between the PMD's orientation and the tangential direction of the target path at each point. Moreover, travel time and the root mean square (RMS) values of the translational and angular speeds were obtained.

B. Results

Fig. 16 shows the experimental driving trajectory with a 60 kg operator, Fig. 17 shows the calculated evaluation metrics, and Fig. 18 shows the experimental scenes.

1) Course 1: The maximum positional RMSE occurred with $\mathcal{L}$ (60 kg), 0.03 m larger than that of $\mathcal{J}$ (Fig. 17(a)) and the maximum angular RMSE occurred with $\mathcal{H}$ (80 kg), 5.16° larger than that of $\mathcal{J}$ (Fig. 17(b)), both negligible for practical driving. These results indicate that the proposed method achieves operability nearly equivalent to $\mathcal{J}$. For the translational speed RMS, $\mathcal{H}$ increases with body weight, whereas $\mathcal{L}$ did not (Fig. 17(d)). This is because $\mathcal{H}$ relies on upper-body weight applied through the hands, while $\mathcal{L}$ depends only on the legs; thus, $\mathcal{L}$'s speed less affected by body weight. For the angular RMSE and angular speed RMS, both peaked at 80 kg for $\mathcal{H}$ or $\mathcal{L}$ (Figs. 17(b), (e)). Heavier users tended to generate larger angular speed when *leaning*, making angular control more difficult. Compared with $\mathcal{J}$, all embodied modes ($\mathcal{H}$, $\mathcal{L}$, and $\mathcal{S}$) showed longer travel times (Fig. 17(c)) and lower translational and angular speeds (Figs. 17(d), (e)). This indicates that while path following is achievable, $\mathcal{H}$ is more fatiguing than $\mathcal{J}$ for long-distance runs, such as Course 1.

2) Course 2: This course showed larger positional and angular RMSEs than the other courses, indicating a stronger influence from uneven ground (Figs. 17(a), (b)). Here, the positional RMSE of all proposed methods was smaller than that of $\mathcal{J}$, while for the angular RMSE, $\mathcal{L}$ showed the largest value, with a difference of 14.9° compared to $\mathcal{J}$. $\mathcal{J}$ also exhibits high RMSEs, so the proposed interface is not uniquely vulnerable on uneven ground.

3) Course 3: The maximum positional RMSE occurred

with $\mathcal{H}$ and $\mathcal{L}$, 0.04 m larger than that of $\mathcal{J}$ (Fig. 17(a)) and the maximum angular RMSE occurred with $\mathcal{H}$ and $\mathcal{S}$, 0.57° larger than that of $\mathcal{J}$ (Fig. 17(b)), both negligible for practical driving. Thus, the proposed interface again provided operability comparable to $\mathcal{J}$. However, differences appear in time and speed: completion time decreased (Fig. 17(c)), and translational/angular speeds increased in the order $\mathcal{H}$, $\mathcal{L}$, $\mathcal{S}$, and $\mathcal{J}$, reflecting ease of operation (Fig. 17(d), (e)). Slope conditions change body posture in $\mathcal{H}$ and $\mathcal{L}$, complicating controlling speeds, i.e., *pressing* and *leaning*. Because the proposed interface relies on body motion as input, posture differences on slopes influence control.

Overall, although the proposed interface required longer completion time than $\mathcal{J}$, it is comparable to $\mathcal{J}$ in its ability to follow the target trajectory and precise speed control.

C. Discussion (limitations and improvements)

1) Force required for input: In this study, a minimum force of around 50 N was required for *press.* In Course 1, this resulted in user fatigue, and in Course 3, operability was sensitive to user's posture changes. Moreover, the system is also difficult to use for individuals unable to exert sufficient force, such as the elderly. The primary cause is the air pressure fluctuation induced by caster rotation (Fig. 7). To address this, in this study, a minimum air pressure was set, inevitably requiring a certain force. Future improvement could include stabilizing the front wheels, for example by changing the wheel type or rigidly connecting the left and right front wheels.

2) Posture of PMD: The proposed interface is strongly affected by how the operator's weight applies force to PMD. In Course 3, changes in the direction of forces on the PMD and the operator degraded operability compared with flat ground, making control more difficult. Moreover, when traveling perpendicular to a slope, the incline shifts the combined CoG of the PMD and operator downslope, causing the airbag to be pressurized even without intentional *pressing* or *leaning*. To address this, the PMD should be equipped with IMUs and adaptively adjust the air pressure thresholds according to road surface condition in future.

3) Pressure threshold value: Currently, pressure thresholds for *press* and *lean* are set experimentally based only on user weight, without considering body shape, muscle mass, or operational skill. Tailoring threshold to individual users would improve usability. We thus plan to implement dynamic updating during operations by applying machine learning techniques [18] to enhance adaptability across diverse users.

VII. Conclusion

This study proposed a control interface where the personal mobility device (PMD) itself serves as the interface by measuring and controlling the airbag pressure of an inflatable PMD. The system recognizes the operator input actions, such as applying force to the PMD body, and adjusts the air pressure based on the estimated operator's weight, enabling operation with minimal force. Continuous speed control was achieved through *press*, *lean*, and *double-push*. Experimental results confirmed that both translational and angular speeds can be controlled by operator's actions. Moreover, filtering effectively mitigated the effects of air pressure fluctuations caused by uneven terrain, ensuring stable operation. Tests on indoor and outdoor courses, including uneven surfaces, demonstrated operability comparable to a joystick, although narrower paths required longer navigation time. These findings highlight the potential of directly integrating the control interface into the PMD, offering a novel approach to PMD control.

In the future, we will evaluate usability of the proposed interface through experiments involving participants with diverse body weights, body shapes, and muscle mass, including elderly and disabled users. We will enhance input recognition resolution and reduce required force by revising the PMD's structural design and applying machine learning systems. We also plan to develop a comfort-adaptive system that adjusts airbag pressure in response to various ground conditions.

References

[1] J. Leaman and H. M. La, "A comprehensive review of smart wheelchairs: past, present, and future," *IEEE Trans. Hum.-Mach. Syst.*, vol. 47, no. 4, pp. 486–499, 2017.

[2] F. W. Siebert, M. Ringhand, F. Englert, M. Hoffknecht, T. Edwards, and M. Rötting, "Braking bad–Ergonomic design and implications for the safe use of shared E-scooters," *Saf. Sci.*, vol. 140, p. 105294, 2021.

[3] H. Zhang and M. N. Norzalilah, "Control strategies for two-wheeled self-balancing robotic systems: a comprehensive review," *Robotics*, vol. 14, no. 8, p. 101, 2025.

[4] H. Sato et al., "Demonstrating poimo as inflatable, inclusive mobility devices with a soft input interface," in *Proc. ACM SIGGRAPH Emerging Technol.*, pp. 1–2, 2022.

[5] R. Niiyama et al., "Poimo: portable and inflatable mobility devices customizable for personal physical characteristics," in *Proc. ACM Symp. User Interface Softw. Technol.*, pp. 912–923, 2020.

[6] H. Sato et al., "Soft yet strong inflatable structures for a foldable and portable mobility," in *Proc. CHI Conf. Hum. Factors Compu. Syst.*, pp. 1–4, 2020.

[7] J. H. Choi, Y. Chung, and S. Oh, "Motion control of joystick interfaced electric wheelchair for improvement of safety and riding comfort," *Mechatronics*, vol. 59, pp. 104–114, 2019.

[8] M. Mrabet, Y. Rabhi, and F. Fnaiech, "Development of a new intelligent joystick for people with reduced mobility," *Appl. Bionics biomech.*, vol. 2018, no. 1, p. 2063628, 2018.

[9] A. Trujillo-León, W. Bachta, J. Castellanos-Ramos, and F. Vidal-Verdú, "Assistive handlebar based on tactile sensors: control inputs and human factors," *Sensors*, vol. 18, no. 8, p. 2471, 2018.

[10] T. Rofer, C. Mandel, and T. Laue, "Controlling an automated wheelchair via joystick/head-joystick supported by smart driving assistance," in *Proc. IEEE Int. Conf. Rehabil. Robot.*, pp. 743–748, 2009.

[11] Y. Chen, D. F. Paez-Granados, M. Hassan, and K. Suzuki, "Torso-based control interface for standing mobility-assistive devices," *IEEE/ASME Trans. Mechatronics*, early access, pp. 1–12, 2024.

[12] J. Woo, K. Yamaguchi, and Y. Ohyama, "Development of a control system and interface design based on an electric wheelchair," *J. Adv. Comput. Intell. Intell. Inform.*, vol. 25, no. 5, pp. 655–663, 2021.

[13] K. Watanabe, R. Yamamura, and Y. Kakehi, "Foamin: A deformable sensor for multimodal inputs based on conductive foam with a single wire," *Ext. Abstr. CHI Conf. Hum. Factors Compu. Syst.*, pp. 1–4, 2021.

[14] Q. Lu, H. Xu, Y. Guo, J. Y. Wang, and L. Yao, "Fluidic computation kit: Towards electronic-free shape-changing interfaces," in *Proc. CHI Conf. Hum. Factors Compu. Syst.*, pp. 1–21, 2023.

[15] C. E. Tejada, R. Ramakers, S. Boring, and D. Ashbrook, "Airtouch: 3d-printed touch-sensitive objects using pneumatic sensing," in *Proc. CHI Conf. Hum. Factors Comput. Syst.*, pp. 1–10, 2020.

[16] Z. Zhang, J. Alvina, F. Détienne, and E. Lecolinet, "Pulling, pressing, and sensing with In-Flat: Transparent touch overlay for smartphones," in *Proc. Int. Conf. Adv. Visual Interfaces*, pp. 1–9, 2022.

[17] H. Nakamura et al., "Hands-free head-motion interface using air pillow," in *Proc. Int. Conf. Intell. Robot. Appl.*, pp. 1–12, 2012.

[18] Y. Huang et al., "Machine learning based skill-level classification for personal mobility devices using only operational characteristics," in *Proc. IEEE/RSJ Int. Conf. Intell. Rob. Syst.*, pp. 5469–5476, 2018.